Cancellation of Distance Measuring Equipment Interference for Aeronautical Communications

Khodr A. Saaifan, Ahmed Elshahed, and Werner Henkel, *Senior Member, IEEE*

***Abstract*—The L-band digital aeronautical communications system (L-DACS1) is subject to strong interference caused by distance measuring equipment (DME). For efficient statistical processing of interference, we adopt a Gaussian mixture (GM) distribution to model the impulsive nature of DME signals. Hence, we drive the parameters of the GM model in terms of properties of DME signals. This allows us to redesign the optimum receiver for mitigating DME interference. We also provide a simple pulse detector to estimate the presence of DME signals utilizing the null subcarriers of L-DACS1.**

***Index Terms*—DME Interference, Gaussian Mixture, L-DACS1, OFDM.**

I. Introduction

The L-band digital aeronautical communications system (L-DACS) technology provides the air-to-ground data link services within the future communications infrastructure (FCI) for aviation. The L-DACS technology identifies two options concerning the operational compatibility with existing systems in the L-band. The first option is L-DACS1, which uses orthogonal frequency division multiplexing (OFDM) modulation with frequency-division duplex (FDD) as an access scheme of the forward and reverse links. The second option, known as L-DACS2, is a narrowband system that uses Gaussian minimum shift keying (GMSK) modulation and the all-purpose multichannel aviation communications system (AMACS) access control.

The multicarrier design of L-DACS1 is more suitable for interference mitigation than L-DACS2 [1]. However, the coexistence of distance measuring equipment (DME) signals in the L-band can interfere significantly with L-DACS1 [2]. To achieve reliable communications, L-DACS1 must employ robust interference mitigation techniques in the physical layer. Due to the impulsive nature of DME pulses, several impulse noise cancellation schemes [3], [4] have been developed in order to mitigate the impact of DME interference [3], [4]. Those methods are classified according to DME suppression either in time or frequency. A clipping and a blanking detector use a memoryless nonlinear operation to either limit or blank the impulse noise affecting received signals [5]. In OFDM systems, the clipping and blanking nonlinearities [6]–[8] are implemented before the fast-Fourier transform (FFT) demodulation. Even though these nonlinearities add almost no complexity to L-DACS1, they require perfect knowledge of DME impaired samples. In frequency domain, there are several algorithms treating the effects of DME interference after the FFT demodulation, such as an erasure-based convolutional decoding strategy and a subcarrier clipping scheme [9], [10]. In [11], [12]; a sparse Bayesian learning (SBL) approach is developed to reconstruct the impacts of impulse noise as a sparse signal. For accurate OFDM demodulation, the maximum-likelihood (ML) decoder utilizes the lattice-like structure the OFDM symbol, which improves the system performance in impulse noise [13], [14]. However, the ML receiver is typically implemented by a lattice decoder, which depends on impulse noise distributions. To redesign the lattice decoder for L-DACS1, we first need to determine sufficient statistical modeling of DME interference at the receiver.

In this paper, we investigate a Gaussian mixture (GM) model to represent the effects of AWGN superimposed to DME interference. We use spectral analysis of received interference to derive the parameters of the GM model in terms of the properties of the DME signals. Then, we develop the lattice decoder of OFDM systems [14] to mitigate the impacts of DME interference. Since lattice decoding requires perfect knowledge of the impulse noise impaired samples. We further make use of the time-frequency properties of the DME signals to efficiently identify their locations within the received OFDM symbols. The rest of this paper is organized as follows: Section II briefly describes the OFDM inlay system of L-DACS1. In Section III, we introduce a GM model to represent DME interference and AWGN at the L-DACS1 receiver. Section IV considers the optimum OFDM receiver of L-DACS1 in the presence of DME interference. Finally, simulation results and concluding remarks are presented in sections V and VI, respectively.

II. L-DACS1 System Model

L-DACS1 is planned to operate in the aeronautical part of the L-band (960-1164 MHz) between adjacent DME channels [15]. Figure 1 illustrates the spectral placement. The aeronautical L-band portion from 960-to-1164 MHz is mainly used by the DME and tactical air navigation (TACAN) systems. DME is a radar system associated with airborne facilities to determine the slant distance of the aircraft to a ground station. The airborne interrogator uses the DME channels in the frequency bands 1041-1083 MHz and 1094-1150 MHz

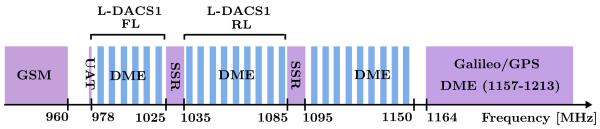

Fig. 1: The spectrum deployment of L-DACS1 in the L-band [15]

K. A. Saaifan and W. Henkel are with the Transmission System Group, Jacobs University Bremen, Bremen, 28759, Germany, e-mail: {k.saaifan, w.henkel}@jacobs-university.de.

to transmit a sequence of Gaussian-shaped pulse pairs. A transponder in the ground station replies with the same sequence of pulses at frequencies ± 63 MHz offset from the interrogation frequency. Hence, the DME channels in a frequency band 978-1025 MHz are only allocated to the responses of ground stations. The inlay approach of L-DACS1 utilizes the gaps in the frequency bands $978-1025$ MHz and $1041-1083$ MHz for the forward and reverse links, respectively. The forward link (FL) is exposed to DME/TACAN interference caused by DME transponders. However, the reverse link (RL) is subject to interference caused by the aircraft interrogator.

A. OFDM System

The FL of L-DACS1 inserts an OFDM system with a bandwidth of 498.05 kHz into the gap between two DME reply channels [15]. The OFDM system is efficiently used to transmit 50 subcarriers with a subcarrier spacing $\Delta f = 9.765625$ kHz. The FFT size $N = 64$ is chosen to provide 7 guard subcarriers on the outer edges of the L-DACS1 spectrum. The OFDM system has a total bandwidth $B_{FFT} = 625$ kHz with an OFDM symbol duration $T = 102.4$ μs. To face different interference conditions, L-DACS1 integrates adaptive modulation and coding (AMC) into the OFDM system. For strong interference conditions, the default setting employs quadrature phase shift keying (QPSK) modulation with concatenated block coding and Reed-Solomon coding in the physical layer. Figure 2 depicts a baseband OFDM system model of L-DACS1. An OFDM symbol can be given as

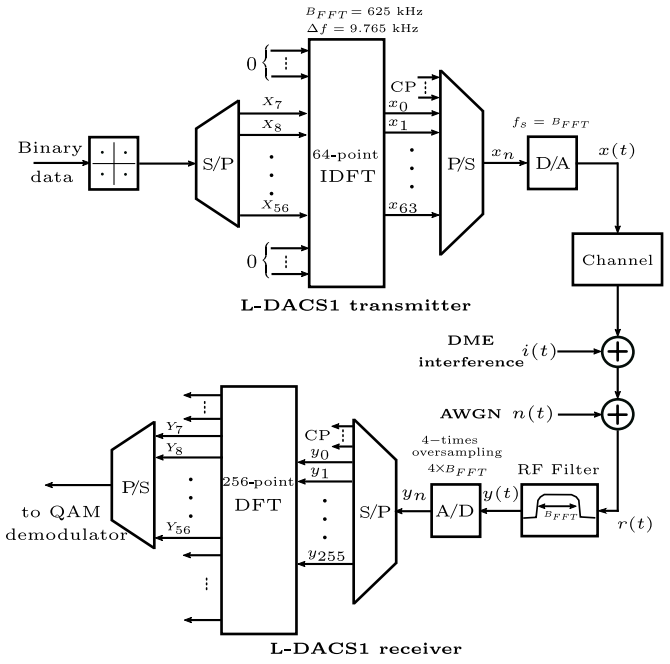

Fig. 2: The L-DACS1 OFDM baseband model

$$x(t) = \sum_{k=7}^{56} X_k e^{j2\pi k \Delta f t}, \quad 0 \le t \le T. \tag{1}$$

where X_k, $k = 7, 8, \cdots, 56$, denote complex-valued data symbols taken from a QAM constellation of a normalized average energy per symbol, $\mathrm{E}\{|X_k|^2\} = 1$. The OFDM symbol is appended by a cyclic prefix (CP) of length 17.6 μs. A part of the CP serves as a guard interval of length 4.8 μs to mitigate the multipath effects of an aeronautical radio channel. The other part is used for transmit windowing to reduce the out-of-band radiation [15]. The baseband received signal can be given as

$$r(t) = \sqrt{\tfrac{E_s}{T}} \sum_{l=0}^{L-1} h_l x(t-\tau_l) + n(t) + i(t), \tag{2}$$

where E_s is the transmitted energy per symbol and T represents the OFDM symbol duration. h_l and τ_l denote the channel coefficient and delay associated with the l^{th} path, respectively. For aeronautical channels, the fading coefficients h_l is a complex-valued random variable. The kind of fading depends on the flight mode of an airborne. The terms $i(t)$ and $n(t)$ represent DME interference and additive white Gaussian noise (AWGN), receptively. For FL transmission, $i(t)$ comprises of reply signals from ground transponders operating in the DME channels at ± 0.5 MHz offset to the enter frequency of the OFDM system. The DME reply signal of the v^{th} ground station consists of a random sequence of Gaussian-shaped pulse pairs with a fixed pulse rate λ_v pulse pairs per second (ppps). The basic DME pulse pair signal can be written as [2]

$$g(t) = e^{-\frac{\alpha}{2}t^2} + e^{-\frac{\alpha}{2}(t-\Delta t)^2}, \tag{3}$$

where $\alpha = 4.5 \cdot 10^{11}$ s^{-2} and Δt is the inter-pulse interval of the two pulses. The DME pulses of the v^{th} ground station at the L-DACS1 receiver are characterized by the peak amplitude A_v and a frequency offset f_v. Since the DME interference observed at the OFDM system is composed of DME pulses from V DME stations, $i(t)$ can be expressed as

$$i(t) = \sum_{v=1}^{V} \sum_{u=1}^{N_v} A_v g(t - t_{v,u}) e^{j2\pi f_v t + j\varphi_{v,u}}, \tag{4}$$

where $N_v = \lambda_v \cdot T$ is the number of DME pulse pairs considered in the OFDM symbol interval T for the v^{th} DME station. The arrival times $t_{v,u}$, $u = 1, \cdots, N_v$ of the v^{th} DME station are randomly generated according to a Poisson random process [2]. The phases $\varphi_{v,u}$ are equally distributed in the interval $[0, 2\pi]$. The RF filter in the IF stage of the L-DACS1 receiver limits only the impacts of DME interference that fall outside the LDACS1 spectrum. The impacts of DME interference that fall within L-DACS1 is given by passing $i(t)$ through a received filter $H_{RF}(f)$. To avoid aliasing effects of DME interference, the received signal after RF filtering is over-sampled by a factor of 4. In a conventional OFDM receiver, the samples of the received signal are transformed into frequency domain by means of an FFT. The length of the FFT is increased according to the over-sampling factor. For further baseband processing, only the subcarriers related to LDACS1 are considered and all other subcarriers are discarded.

B. Aeronautical Channel Models

The different flight modes of the aircraft lead to several distinct wireless channel scenarios for L-DACS1. The channel

model [16], [17] of each scenario is characterized by the type of fading, the Doppler frequency f_D, and the delay spread τ. In Table I, we summarize the channel models for different worst-case scenarios such as en-route, take-off/landing, and parking [17]. The en-route and take-off/landing scenarios

TABLE I: Channel model parameters for different flight scenario [17]

Scenario	fading	delay spread	Doppler frequency
en-route	Ricean, Rice factor $K_R = 15$ dB	direct + 2 paths $\tau_1 = 0.4$ μs and $\tau_2 = 15.2$ μs	Gaussian PSD, $f_D = 1.25$ kHz
take-off/landing	Ricean, Rice factor $K_R = 10$ dB	exponential, $\tau_{\max} = 20$ μs	Jakes PSD, $f_D = 512$ Hz
parking	Rayleigh	exponential, $\tau_{\max} = 3$ μs	Jakes PSD, $f_D = 54.6$ Hz

correspond to the case where a very strong line-of-sight (LOS) direct path is present between the ground station and the aircraft. Since the L-DACS1 receiver is assumed to be perfectly synchronized with the delay spread and Doppler shift, the receive signal can be written as

$$r(t) = \sqrt{\frac{E_s}{T}} h_0 x(t) + n(t) + i(t) \,, \tag{5}$$

where h_0 is a constant gain of the channel. Due to the strong LOS component, the performance of L-DACS1 for the en-route scenario is similar to the performance of the additive interference plus noise channel. In the parking scenario, the channel model can be approximated by frequency-selective Rayleigh fading with an exponential power delay profile [17].

III. Statistical Models for DME interference

One of the essential steps for receiver optimization in interference limited channels is the statistical modeling of the received interference. For Gaussian interference, the optimum OFDM receiver can be implemented using the FFT receiver. However, when the interference exhibits an impulsive appearance, the FFT algorithm is not optimum for OFDM signal detection in impulse noise [13]. The impulsive nature of DME signals follows some heavy-tailed distributions. Existing models of impulse noise are classified as either empirical or statistical-physical. On the one hand, empirical models provide tractable distributions, which fit the probability distributions of measured data. On the other hand, the statistical-physical models admit more accurate and complex distributions whose parameters have a direct physical significance. In the following subsections, we adopt a GM distribution to model the influence of DME interference superimposed to AWGN. Additionally, we evaluate a power spectral density of DME signals to derive the parameters of the GM model.

A. Gaussian Mixture Model

A GM distribution is one of the most accepted models for impulse noise superimposed to AWGN [18], [19]. The GM model is designated to approximate a Middleton Class-A (MCA) model for moderate and strong impulse noise environments [20]. Similar to received interference at L-DACS1, the MCA model [21] assumes that the received interference $z(t)$ consists of two independent components: a Gaussian component $n(t)$ and an impulsive component $i(t)$. The impact of $i(t)$ can be represented as a train of random pulses as illustrated in Fig. 3. The impulsive waveforms comprising $i(t)$ have the

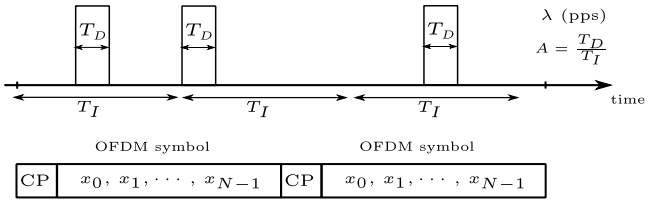

Fig. 3: OFDM signals in the presence of impulse noise

same impulse duration T_D, which is quite similar to the DME signals. According to the rate of impulses $\lambda = 1/T_I$, the duty cycle $A = \frac{T_D}{T_I}$ defines the impulsive index of the MCA model. The GM approximation of the MCA model assumes that the samples of $i(t)$ follow a Gaussian distribution with variance $\sigma_I^2 = \mathrm{E}\{i(t)\}$. For $A < 1$, the probability distribution of the complex-valued received interference $z(t) = n(t) + i(t)$ can be expressed as [22]

$$p_z(z) = \frac{1-A}{\pi\sigma_0^2} e^{-\frac{|z|^2}{\sigma_0^2}} + \frac{A}{\pi\sigma_1^2} e^{-\frac{|z|^2}{\sigma_1^2}} \,, \tag{6}$$

where

$$\sigma_m^2 = \sigma_G^2 + \frac{m}{A}\sigma_I^2 \,, \quad m = 0,\, 1 \,, \tag{7}$$

where σ_G^2 denotes the variance of complex-valued Gaussian noise $n(t)$. The ratio $\Upsilon = \frac{\sigma_G^2}{\sigma_I^2}$ represents the Gaussian factor of the MCA model. The GM approximation considers that the noise process of $z(t)$ has two states $m = 0$ and $m = 1$. The Gaussian state $m = 0$ denotes AWGN and $m = 1$ indicates the presence of impulse noise. The variance of $z(t)$ can be expressed as

$$\begin{aligned} \sigma^2 &= (1-A)\sigma_0^2 + A\sigma_1^2 \,, \\ &= \sigma_G^2 + \sigma_I^2 \,. \end{aligned} \tag{8}$$

This model is memoryless since the impulsive samples are taken independently according to a state probability A. In OFDM systems, the received OFDM signal is typically sampled at a frequency $f_s = B_{FFT}$. Since the duration of pulsed interference $T_D \geq 1/B_{FFT}$, the impulsive samples corrupt a few consecutive samples of the received OFDM symbol. For DME interference, T_D may reach 20% of the length of the OFDM symbol [23]. A Markov model can be well integrated into a memoryless GM model to introduce memory between impulse noise samples [22]. The probability distribution of the received noise sample z_n under a known state of noise m_n can be given as

$$p_z(z_n|m_n) = \frac{1}{\pi\sigma_{m_n}^2} e^{-\frac{|z_n|^2}{\sigma_{m_n}^2}} \,, \tag{9}$$

which is the same for impulse noise models with and without memory. However, for impulse noise with memory, the receiver can utilize the correlation properties of impulsive waveforms to identify the presence of impulses. To specify an accurate model for DME interference, one should relate the GM parameters A and Υ to the proprieties of DME pulses.

B. Spectral Analysis and Parameters Determination

As already mentioned, the baseband DME interference at the L-DACS1 receiver is obtained by passing $i(t)$ through an RF filter. The noise resulting from passing AWGN and DME interference through a band-limiting receive filter can be expressed by

$$\grave{z}(t) = \grave{n}(t) + \grave{i}(t)\,, \tag{10}$$

where $\grave{n}(t)$ and $\grave{i}(t)$ are the contributions of AWGN and DME interference inside the L-DACS1 spectrum, respectively. The samples of $\grave{n}(t)$ can be modeled as band-limited complex-valued white Gaussian noise with zero mean and variance $\sigma_G^2 = N_0 B_{FFT}$. To derive the GM parameters A and Υ of DME interference, we first consider the interference $i_v(t)$ of the v^{th} DME station operating at a frequency offset $f_v = B_{FFT}/2 - 0.5$ MHz. Then, we extend the result to derive the impacts of V DME stations operating at the same or different offset frequencies. Figure 4 illustrates a baseband model and signal processing of DME interference at the L-DACS1 receiver. Due to the cyclostationary feature of the

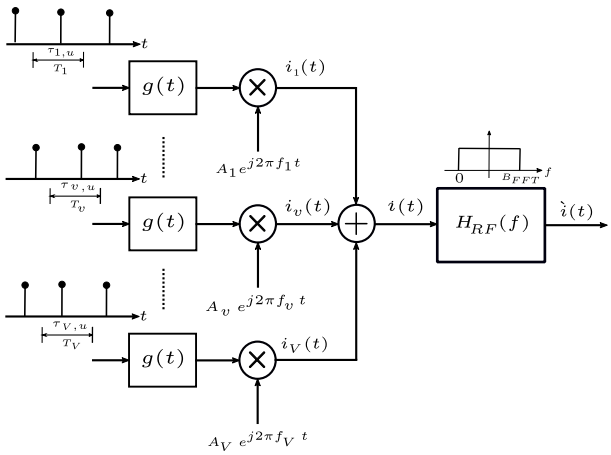

Fig. 4: A baseband model of DME interference for L-DACS1

DME pulses, $i_v(t)$ can be expressed as

$$i_v(t) = A_v \sum_{u=-\infty}^{\infty} g(t - uT_v - t_{v,u}) e^{j2\pi f_v t + j\varphi_{v,u}}\,, \tag{11}$$

where $T_v = 1/\lambda_v$ is the period of pulses and delays $t_{v,u}$, $\forall u$, are uniformly distributed in the range with $[0, T_v]$. Since $g(t)$ is deterministic, the time-average power spectral density of $i_v(t)$ can be written as

$$S_{i_v}(f) = \frac{A_v^2}{T_v} |G(f - f_v)|^2\,, \tag{12}$$

where $G(f)$ is the Fourier transform of $g(t)$, which is

$$G(f) = 2\sqrt{\frac{2\pi}{\alpha}} e^{-\frac{2\pi^2}{\alpha} f^2} \cos(\pi f \Delta t) e^{-j\pi f \Delta t}\,, \tag{13}$$

where $\Delta t = 12\,\mu$s for the X-mode operation of the DME station. Since $i_v(t)$ is passed through a receive filter $H_{RF}(f)$, the time-average power spectral density of the filtered interference, $\grave{i}_v(t)$, is given by

$$S_{\grave{i}_v}(f) = \frac{A_v^2}{T_v} |G(f - f_v)|^2 |H_{RF}(f)|^2\,. \tag{14}$$

Figure 5 depicts the time-average power spectral density of DME pulses at the offset frequency $B_{FFT}/2 - 0.5$ MHz with $A_v = 1$ and $\lambda_v = 3600$ ppps. Ideally, the received filter

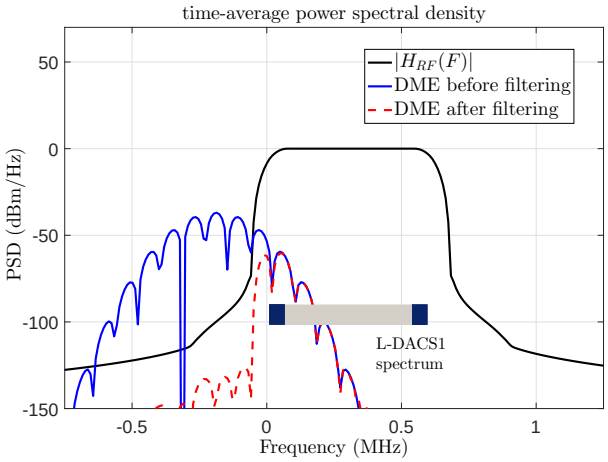

Fig. 5: The spectrum of DME interference operating at -0.5 MHz offset to the center frequency of L-DACS1

$H_{RF}(f)$ should pass the baseband spectrum of L-DACS1, i.e., $H_{RF}(f) = 1$ for $0 \le f \le B_{FFT}$. The time-average autocorrelation function can be expressed as

$$\begin{aligned}\phi_{\grave{i}_v}(\tau) &= \int_{-\infty}^{\infty} S_{\grave{i}_v}(f) e^{j2\pi f\tau} df\,,\\ &= \tfrac{A_v^2}{T_v} \int_0^{B_{FFT}} |G(f - f_v)|^2 e^{j2\pi f\tau} df\,.\end{aligned} \tag{15}$$

Indeed, the received DME interference $\grave{i}(t)$ comprises of multiple DME random sequences from different and independent DME ground stations. Thus, the time-average power spectral density of DME interference caused by V DME stations can be given as

$$S_{\grave{i}}(f) = \sum_{v=1}^{V} \frac{A_v^2}{T_v} |G(f - f_v)|^2 |H_{RF}(f)|^2\,. \tag{16}$$

Since the background Gaussian noise $\grave{n}(t)$ and DME interference are statistically independent, the time-average power spectral density of the received interference $\grave{z}(t)$ is

$$S_{\grave{z}}(f) = N_0 \cdot \text{rect}\left(\frac{f - \frac{B_{FFT}}{2}}{B_{FFT}}\right) + S_{\grave{i}}(f)\,. \tag{17}$$

The variance of $\grave{z}(t)$ can be computed as

$$\begin{aligned}\sigma^2 &= \int_0^{B_{FFT}} S_{\grave{z}}(f) df\,,\\ &= N_0 \cdot B_{FFT} + \sum_{v=1}^{V} \tfrac{A_v^2}{T_v} E_{g,v}\,.\end{aligned} \tag{18}$$

where $E_{g,v} = \int_0^{B_{FFT}} |G(f - f_v)|^2 df$. The term $N_0 \cdot B_{FFT}$ denotes the variance of AWGN, σ_G^2. From (18) and (8), the variance σ_I^2 can be related to the properties of DME interference as

$$\sigma_I^2 = \sum_{v=1}^{V} \frac{A_v^2}{T_v} E_{g,v}\,. \tag{19}$$

Since the DME random sequences of the V ground stations are independent, the pulse rate of the composite sequence is $\lambda_I = \sum_{v=1}^{M} \lambda_v$. This is in agreement with a Poisson process for modeling and simulating DME interference. Thus, the duty cycle of composite pulses is

$$\begin{aligned} A &= \frac{T_D}{T_I}\,, \\ &= \lambda_I T_D\,, \end{aligned} \tag{20}$$

where T_D is the duration of the basic DME pulse after filtering and $T_I = 1/\lambda_I$ is the average period of the composite DME pulses.

To investigate the amplitude distributions of the received interference $\grave{z}(t)$, we consider a worst-case scenario for DME interference [9], [10]. In such a case, the receiver is exposed to a strong DME station operating at $f_1 = B_{FFT}/2 - 0.5$ MHz with a peak power of -67.9 dBm. The received signal is additionally corrupted by another DME station at $f_2 = B_{FFT}/2 + 0.5$ MHz with a peak power of -74 dBm. The pulse rate of each station is $\lambda_{1,2} = 3600$ ppps. Figure 6 illustrates the composite DME pulses $\grave{i}(t)$. Since the interference process

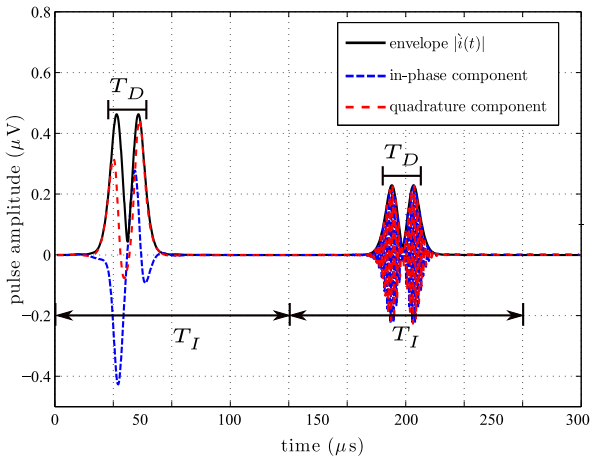

Fig. 6: The impulsive appearance of DME interference at the L-DACS1 receiver

is complex-valued, we depict the envelope and quadrature components of $\grave{i}(t)$. For both DME stations, the basic DME pulse pair after filtering is characterized by $T_D = 20$ μs and $E_{g,v} = 1.6 \cdot 10^{-8}$ W/Hz. In Table II, we summarize the properties of DME interference for the worst-case scenario. For additive Gaussian noise, we assume the thermal noise

TABLE II: The properties of DME pulses after the receive filter

Scenario	T_D (μs)	λ_v (ppps)	A_v (μV)	$E_{g,v}$ (W/Hz)
DME station 1	20	3600	12.735	1.6×10^{-8}
DME station 2	20	3600	6.301	1.6×10^{-8}

density $N_0 = -174$ dBm/Hz, which results in a noise power $\sigma_G^2 = 2.49 \times 10^{-15}$ W in the considered bandwidth

TABLE III: The parameters of the GM model for the worst-case scenario of DME interference

λ_I (ppps)	$A = \lambda_I \times T_D$	σ_I^2 (W)	$\Upsilon = \frac{\sigma_G^2}{\sigma_I^2}$
7200	0.144	1.165×10^{-14}	0.2135

$B_{FFT} = 625$ kHz. According to the values in Table II, we use (19) and (20) to compute the parameters of the GM model as presented in Table III. To demonstrate the GM model of $\grave{z}(t)$, we computed the probability density function (PDF) for the amplitudes of the in-phase and quadrature components. Figure 7 depicts the GM distribution for modeling the received interference. We observe that the GM distribution provides

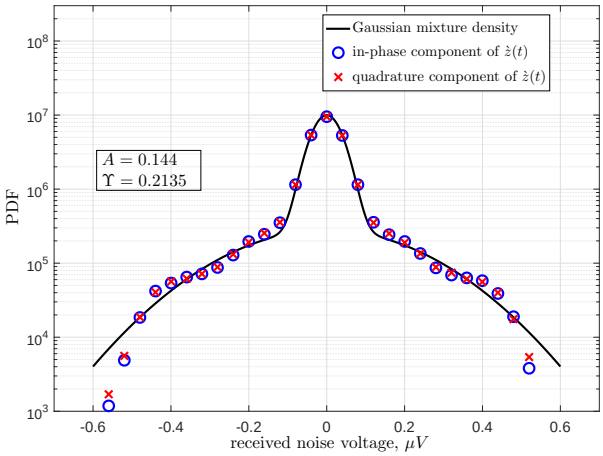

Fig. 7: The GM distribution of the received DME interference caused by two DME stations for the en-route scenario

a sufficient model for DME interference and AWGN. In addition, we observe that $\sigma_I^2 \gg \sigma_G^2$, which justifies the heavy tails of the computed PDF. The previous analysis is well-suited to aeronautical channels with a strong LOS component. Similar to the L-DACS1 channels, the DME signal from each DME station is transmitted over an aeronautical channel with different scenarios. In a parking scenario, the received interference in multipath fading channels is

$$i(t) = \sum_{v=1}^{V} \sum_{l=0}^{L-1} h_{v,l}\, i_v(t - \tau_{v,l})\,, \tag{21}$$

where $h_{v,l}$, $\forall l$, are complex-valued Gaussian distributed channel coefficients. The average power of the v^{th} DME channel is given by $\sigma_{hv}^2 = \sum_{l=0}^{L-1} \mathrm{E}\left\{|h_{v,l}|^2\right\}$. Hence, the variance σ_I^2 (cf. (19)) can be rewritten as

$$\sigma_I^2 = \sum_{v=1}^{V} \frac{A_v^2 \sigma_{hv}^2}{T_v} E_{g,v}\,, \tag{22}$$

which extends the GM model to represent DME interference with fading. In Fig. 8, we investigate the PDF of the received DME interference through a two-path fading channel. For simplicity, we assume two equal power paths with $\sigma_{hv}^2 = 1$ and $\tau_{max} = 3$ μs. Since $\tau_{max} \ll T_D$, it is interesting to note

that the GM modeling of (21) provides the same parameters of DME interference as without fading.

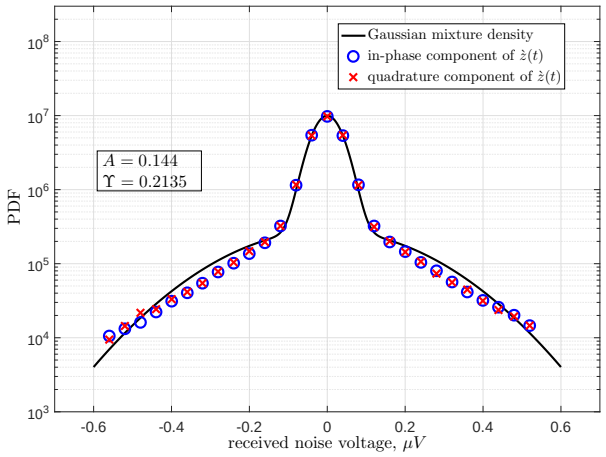

Fig. 8: The GM distribution of the received fading DME interference for a parking scenario

IV. Receiver Design and Optimization

The detection problem of OFDM signals involving a GM model for impulse noise is considered in [14]. The optimum detector treats the OFDM symbol as a complex number (CN) code that uses the IDFT matrix as a generator matrix [13]. The design rule of the CN codes in memoryless GM noise shows that the IDFT mapping provides a large coding gain. Since the existence of a DME pulse within an OFDM symbol corrupts several consecutive received samples, a memoryless assumption for DME pulses will not be correct. Hence, to optimize the L-DACS1 receiver, we need to specify the joint distribution of the impaired samples by DME pulses. At the L-DACS1 receiver, the received OFDM symbol after filtering can be expressed as follows:

$$y(t) = \sqrt{\frac{E_s}{T}} \sum_{l=0}^{L-1} h_l x(t-\tau_l) + \dot{z}(t)\,, \tag{23}$$

where $\dot{z}(t) = \dot{n}(t) + \dot{i}(t)$ can be modeled by the GM distribution with parameters σ_G^2, A, and σ_I^2 as presented in the previous section. To avoid aliasing of DME interference occurring at offset frequencies outside the OFDM bandwidth, the received signal is over-sampled by sampling rate $f_s^{\text{ov}} = 4 \cdot B_{FFT}$. The received samples within an OFDM symbol can be expressed as

$$y_{n_s} = \sum_{n_s=0}^{255} \delta(t - n_s T_s^{\text{ov}}) y(t)\,, \quad 0 \le t \le T\,, \tag{24}$$

where $T_s^{\text{ov}} = \frac{1}{4 \cdot B_{FFT}}$ is the sample spacing. From (23) and (24), we obtain

$$y_{n_s} = \sqrt{\frac{E_s}{T}} \sum_{l=0}^{L-1} h_l x[n_s - \mu_l] + \dot{z}_{n_s}\,,\ n_s = 0, \cdots, 255\,, \tag{25}$$

where $\mu_l = [\tau_l / T_s^{\text{ov}}]$ is the channel delay (rounded to samples) associated with the l^{th} path. The sample index $[n_s - \mu_l]$ for $n_s = 0, \cdots 255$ represents $[n_s - \mu_l]$ modulo 256 due to the CP insertion. Since $T = 256 \cdot T_s^{\text{ov}}$, the received OFDM symbol consist of $N_s = 256$ samples. In a matrix form, the received OFDM vector can be expressed as

$$\mathbf{y} = \sqrt{\frac{E_s}{N_s T_s^{\text{ov}}}} \bar{\mathbf{H}} \mathbf{F}_{N_s}^H \mathbf{X} + \dot{\mathbf{z}}\,, \tag{26}$$

where $\bar{\mathbf{H}} \in \mathbb{C}^{N_s \times N_s}$ is a circulant convolution channel matrix of i.i.d. complex Gaussian entries. The matrix $\mathbf{F}_{N_s}^H$ denotes the inverse discrete Fourier transform matrix. Since $\mathbf{W}_{N_s}^H = \frac{1}{\sqrt{N_s}} \mathbf{F}_{N_s}^H$ forms a unitary IDFT matrix, the received OFDM vector can be given by

$$\mathbf{y} = \sqrt{\frac{E_s}{T_s^{\text{ov}}}} \bar{\mathbf{H}} \mathbf{x} + \dot{\mathbf{z}}\,, \tag{27}$$

where the OFDM symbol $\mathbf{x} = \mathbf{W}_{N_s}^H \mathbf{X}$ results from an IDFT of a complex-valued data vector $\mathbf{X} = [X_0, \cdots, X_{255}]^T$, which contains the transmit data symbols X_k, $k = 7, \cdots, 56$. Due to over-sampling, the received interference vector $\dot{\mathbf{z}} \in \mathbb{C}^{256 \times 1}$ spreads the samples of DME interference on $N_I = \lceil T_D / T_s^{\text{ov}} \rceil = 50$ consecutive observations. Similar to (9), the probability distribution of $\dot{z}_{n_s}$, $n_s = 0, \cdots, 255$, under perfect knowledge of impaired samples by DME interference, is

$$p_z(\dot{z}_{n_s}) = \begin{cases} \frac{1}{\pi \dot{\sigma}_0^2} \mathrm{e}^{-\frac{|\dot{z}_{n_s}|^2}{\dot{\sigma}_0^2}}\,, & \text{if } \overbrace{\dot{z}_{n_s} = \dot{n}_{n_s}}^{m_{n_s}=0}\,, \\ \frac{1}{\pi \dot{\sigma}_1^2} \mathrm{e}^{-\frac{|\dot{z}_{n_s}|^2}{\dot{\sigma}_1^2}}\,, & \text{if } \overbrace{\dot{z}_{n_s} = \dot{n}_{n_s} + \dot{i}_{n_s}}^{m_{n_s}=1}\,, \end{cases} \tag{28}$$

where $\dot{n}_{n_s}$ denotes a sample of band-limited complex-valued Gaussian noise $\dot{n}(t)$ with variance $\sigma_G^2 = N_0 \cdot B_{FFT}$ in the L-DACS1 bandwidth B_{FFT}. The impaired samples by DME interference $\dot{z}_{n_s} = \dot{n}_{n_s} + \dot{i}_{n_s}$ can be modeled as Gaussian noise with variance $\dot{\sigma}_1^2 = \sigma_G^2 + \frac{1}{A}\sigma_I^2$, where σ_I^2 and A are computed by (19) and (20), respectively. The temporal correlation of the DME signal determines the covariance matrix of the noise observations, which leads to an N_s-dimensional GM model [24]. Hence, under perfect knowledge of noise states, the distribution of the received interference vector $\dot{\mathbf{z}}$ can be written as

$$p(\dot{\mathbf{z}}) = \frac{1}{\pi^{N_s} |\mathbf{\Sigma}_{\dot{\mathbf{z}}}|} e^{-\dot{\mathbf{z}}^H \mathbf{\Sigma}_{\dot{\mathbf{z}}}^{-1} \dot{\mathbf{z}}}\,, \tag{29}$$

where $\mathbf{\Sigma}_{\dot{\mathbf{z}}}$ is the covariance matrix of $\dot{\mathbf{z}}$. In the absence of DME signals, the covariance matrix can be given as $\mathbf{\Sigma}_{\dot{\mathbf{z}}} = \sigma_G^2 \mathbf{I}_{N_s}$. However, in the presence of DME interference within the received OFDM symbol, we need to evaluate the exact covariance matrix of the DME samples. For simplicity, we design the optimum L-DACS1 receiver with

$$\begin{aligned} \mathbf{\Sigma}_{\dot{\mathbf{z}}} &= \mathrm{E}\left[\dot{\mathbf{z}} \dot{\mathbf{z}}^H\right]\,, \\ &= \begin{pmatrix} \dot{\sigma}_{m_0}^2 & 0 & \cdots & 0 \\ 0 & \dot{\sigma}_{m_1}^2 & \cdots & 0 \\ \vdots & \vdots & \ddots & \vdots \\ 0 & 0 & \cdots & \dot{\sigma}_{m_{N_s-1}}^2 \end{pmatrix}\,, \end{aligned} \tag{30}$$

where m_{n_s}, $n_s = 0 \cdots N_s - 1$, are noise states of the interference observations $\grave{z}_{n_s}$ within the received OFDM symbol. Thus, $m_{n_s} = 0$ for samples corrupted only by AWGN and $m_{n_s} = 1$ for impaired samples by DME interference. The above model represents the samples of DME interference as independent Gaussian random variables. To model the temporal correlation of DME samples, $\mathbf{\Sigma}_{\grave{\mathbf{z}}}$ should include correlation coefficients outside the main diagonal. In the following subsections, we introduce a simple DME pulse detector to determine the noise states of DME interference. Then, we present the optimum OFDM receiver to mitigate the effects of DME interference.

A. DME Pulse Detection

The detection of DME pulses was considered in [8], [25] to limit the impact of impaired samples together with a pulse clipping technique. The locations of DME samples are identified using a correlation with a Gaussian-shaped pulse. This approach exploits the shape of the DME pulses to indicate the presence of DME interference. However, the correlation approach suffers from false detection of DME pulses at high signal levels. To overcome this problem, we make use of the guard subcarriers of the OFDM system to reconstruct a reference signal of the interference. After an FFT block, i.e., $\mathbf{Y} = \mathbf{W}_{N_s}\mathbf{y}$, the received signal from the null subcarriers is given by [8]

$$Y[k] = \grave{N}[k] + \grave{I}[k]\,, \quad k = 0, \cdots, 6, 57, \cdots 63\,, \tag{31}$$

where $\grave{N}[k]$ and $\grave{I}[k]$ represent the DFT samples of AWGN and DME interference, respectively. Since the power spectral density of DME interference is concentrated at the edges of the L-DCAS1 spectrum, the null subcarriers of the OFDM system are sufficient to reconstruct a replica of received interference. Therefore, one can reconstruct a reference signal of the interference as

$$\grave{\mathbf{z}}_{\text{ref}} = \mathbf{W}_{N_s}^{H}\mathbf{Y}_{\text{null}}\,, \tag{32}$$

where $\mathbf{Y}_{\text{null}} \in \mathbb{C}^{256\times 1}$ is formed only by the data of null subcarriers, $Y_{\text{null},k} = R_k$, $k = 0, \cdots, 6, 57, \cdots 63$. Figure 9 depicts a received OFDM signal and a reference replica of the interference employing the null subcarriers of the OFDM system. The power level of the received signal was set such that the signal-to-noise ratio, E_s/N_0, is equal to 10 dB. Similar to the correlation approach, we correlate $\grave{\mathbf{z}}_{\text{ref}}$ with a generic Gaussian-shaped pulse. The generic DME pulse in discrete time is given by

$$d[k] = e^{-\frac{\alpha}{2}(k/f_s^{\text{ov}})^2}\,, \quad k = 0, \cdots, N_s - 1\,. \tag{33}$$

The cross-correlation $\grave{\mathbf{z}}_{\text{cr}}$ between the time domain reference signal $\grave{\mathbf{z}}_{\text{ref}}$ and a generic DME pulse can be expressed as

$$\grave{z}_{\text{cr}}[n_s - k] = \mathrm{E}\left\{\grave{z}_{\text{ref}}[n_s]d^*[k]\right\}\,. \tag{34}$$

Based on a cross-correlation signal, a threshold decision can efficiently identify the locations of DME pulses. Figure 10 illustrates a cross-correlation signal of the reference interference with the generic Gaussian-shaped pulse. From this figure, we observe that the peaks of the cross-correlation signal

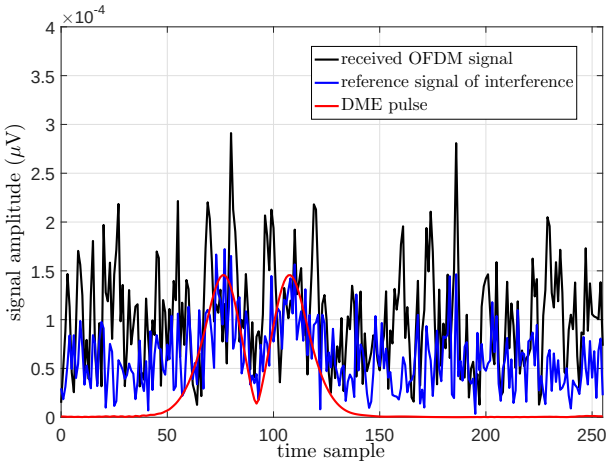

Fig. 9: Utilizing the null subcarriers to extract a reference signal of received interference

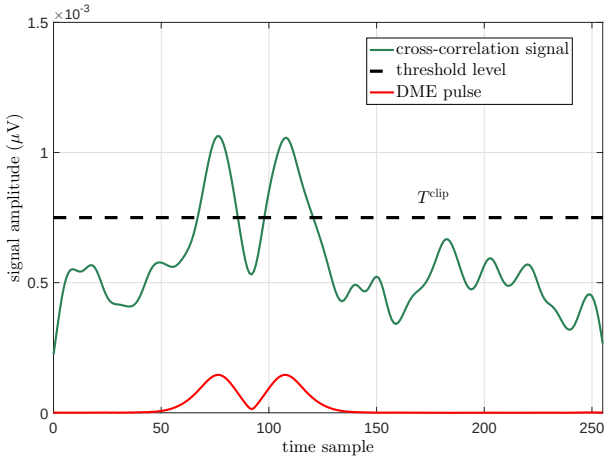

Fig. 10: DME pulse detection from a cross-correlation signal

completely match the peaks of the actual DME interference. This leads to efficient detection of DME pulses regardless to the power of the received OFDM signal. To compute the covariance matrix $\mathbf{\Sigma}_{\grave{\mathbf{z}}}$ of noise observations, the noise states m_{ns} can be estimated as

$$m_{n_s} = \begin{cases} 1 & \text{for } |\grave{z}_{\text{cr}}[n_s]| \geq T^{\text{clip}}\,, \\ 0 & \text{for } |\grave{z}_{\text{cr}}[n_s]| < T^{\text{clip}}\,, \end{cases} \tag{35}$$

where T^{clip} denotes a clipping threshold to identify the DME pulses [25].

B. Optimum OFDM Receiver

Using the N_s-dimensional GM model (29), the likelihood functions $p(\mathbf{y}|\mathbf{X})$ of the received signal (27) can be expressed as

$$p(\mathbf{y}|\mathbf{X}) = \frac{1}{\pi^{N_s}|\mathbf{\Sigma}_{\grave{\mathbf{z}}}|} e^{-\left(\mathbf{y}-\sqrt{\frac{E_s}{T_s^{\text{ov}}}}\bar{\mathbf{H}}\mathbf{x}\right)^H \mathbf{\Sigma}_{\grave{\mathbf{z}}}^{-1}\left(\mathbf{y}-\sqrt{\frac{E_s}{T_s^{\text{ov}}}}\bar{\mathbf{H}}\mathbf{x}\right)}\,. \tag{36}$$

Similar to the optimum OFDM detector in GM noise, we optimize the L-DACS1 receiver to select the sequence that

maximizes $p(\mathbf{y}|\mathbf{X})$. For M-ary modulation schemes and N_d used subcarriers, the receiver searches over M^{N_d} possible choices of the transmitted signal vector $\mathbf{X}$. For L-DACS1 with QPSK, the optimum receiver searches over 4^{50} possible sequences. Since $\mathbf{\Sigma}_{\tilde{\mathbf{z}}}^{-1} = \mathbf{L}\mathbf{L}^H$, where $\mathbf{L} = \mathrm{diag}\left[1/\sigma_{m_0}, \cdots, 1/\sigma_{m_{N_s-1}}\right]$, the maximum likelihood (ML) estimate of the transmitted symbol leads to

$$\hat{\mathbf{X}}_{\mathrm{ML}} = \arg\min_{\mathbf{X}} \left|\mathbf{L}^H\mathbf{y} - \sqrt{\tfrac{E_s}{T_s^{\mathrm{ov}}}}\mathbf{L}^H\bar{\mathbf{H}}\mathbf{W}_{N_s}^H\mathbf{X}\right|^2 , \qquad (37)$$

which searches over all possible information symbols to select a closest signal vector to the received vector $\mathbf{L}^H\mathbf{y}$. To avoid the exhaustive search of the optimum receiver, we use a sphere decoder, which searches only over possible lattice points that lie within a sphere of radius β_0. The sphere equation of the optimum detector can be expressed as

$$\left|\mathbf{L}^H\mathbf{y} - \mathbf{G}\mathbf{X}\right|^2 \leq \beta_0 , \qquad (38)$$

where $\mathbf{G} = \sqrt{\tfrac{E_s}{T_s^{\mathrm{ov}}}}\mathbf{L}^H\bar{\mathbf{H}}\mathbf{W}_{N_s}^H$. The sphere equation (38) can be implemented sequentially as in [26], or concurrently as in [27], [28]. Using a QR decomposition, the matrix $\mathbf{G}$ can be factorized into a product of a unitary matrix $\mathbf{Q}$ and an upper triangular matrix $\mathbf{R}$. Thus, (38) can be reduced as

$$\begin{aligned} \left|\mathbf{L}^H\mathbf{y} - \mathbf{Q}\mathbf{R}\mathbf{X}\right|^2 &\leq \beta_0 , \\ \left|\mathbf{Q}^H\mathbf{L}^H\mathbf{y} - \mathbf{Q}^H\mathbf{Q}\mathbf{R}\mathbf{X}\right|^2 &\leq \beta_0 , \\ \left|\mathbf{y}^{'} - \mathbf{R}\mathbf{X}\right|^2 &\leq \beta_0 , \end{aligned} \qquad (39)$$

which is identical to solving the following linear least squares problem

$$\sum_{n=n_s}^{N_s-1} \left|y_n^{'} - \textstyle\sum_{k=n}^{N_s-1} R_{n,k}X_k\right|^2 \leq \beta_0 , n_s = N_s - 1, \cdots, 0 . \qquad (40)$$

For L-DACS1, the sphere decoder solves the above set of conditions in the order of $n_s = 56$ to $n_s = 7$.

V. Simulation Results

We performed a link level simulation to validate the receiver optimization of L-DACS1 in canceling the effects of DME interference. To assess the receiver performance, we implemented the described DME detection scheme along with the sphere decoder to realize the optimum OFDM receiver.

For generating the OFDM signal, uncoded QPSK symbols were transmitted over an AWGN channel for the en-route scenario. However, to investigate the performance of L-DACS1 in the parking scenario, we consider a Rayleigh fading channel. For both scenarios, we first consider the worst-case for the DME interference. Then, we investigated the case of a single DME station on the L-DACS1 spectrum with a received peak power -65 dBm and different rates of pulses. We use (19) and (20) to determine the GM parameters for each case. In the following results, we depicted a bit-error ratio (BER) versus E_s/N_0 of the sphere decoder compared with the clipping detector and the conventional OFDM receiver. For comparison, the performances obtained for AWGN and memoryless GM noise are also depicted as references. Figure 10 shows the BER curves for the en-route channel in the presence of DME interference caused by two different DME ground stations as given in Table II. For this scenario, we additionally depict the performance of the optimum receiver in memoryless GM noise with the predetermined parameters $A = 0.144$ and $\Upsilon = 0.2135$ as a reference. Second, we repeated the simulations

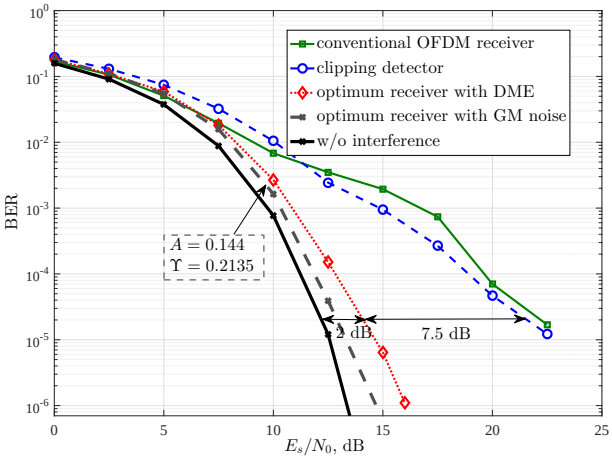

Fig. 11: Performance comparisons of different L-DACS1 receivers for two DME interferers, QPSK, uncoded, and an AWGN channel.

to investigate the performance of the optimum receiver in the parking scenario as illustrated in Fig. 12. For simplicity, we assume flat Rayleigh fading. From both figures, we observe

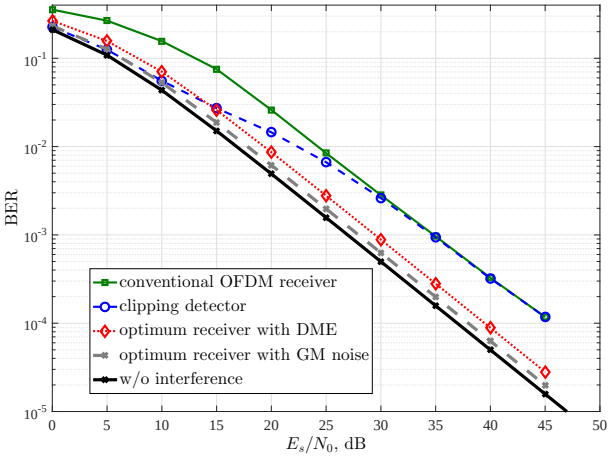

Fig. 12: Performance comparisons of different L-DACS1 receivers for two DME interferers, QPSK, uncoded, and a Rayleigh fading channel.

that the optimum receiver provides better performance than the conventional receiver and the clipping detector. Additionally, we observe that the optimum receiver for DME interference provides a performance near the limit of GM noise. This confirms the robustness of the optimum receiver against the impulsive nature of DME interference as well.

Figure 13 depicts the BER curves for the en-route scenario in the presence of one DME interferer with power -65 dBm

and different pulse rates $\lambda_I = 10800$ ppps, $\lambda_I = 7200$ ppps, and $\lambda_I = 3600$ ppps. This scenario results in different values of the parameters A and Υ of GM noise. From (19) and (20), for a fixed DME power, we note that σ_I^2 and A are increased as the pulse rate increases. This justifies why the optimum receiver provides different performances with respect to the rate of pulses.

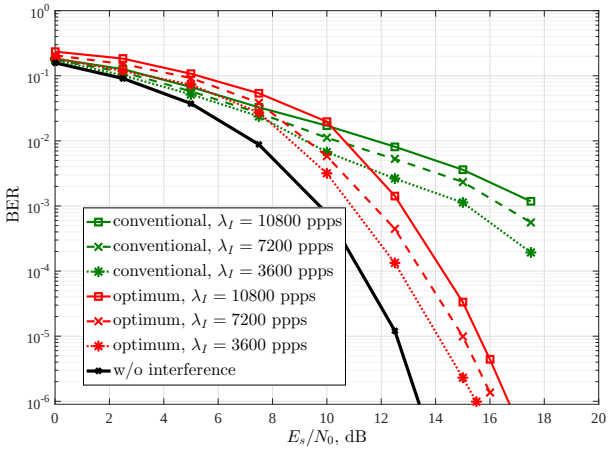

Fig. 13: Performance comparisons for a single DME interferer with different pulse rates, QPSK, uncoded, and an AWGN fading channel.

VI. Conclusion

In this paper, we have investigated the statistical modeling and cancellation of distance measuring equipment (DME) interference for the L-band digital aeronautical communication system (L-DACS1). In particular, we treat the impacts of DME interference as impulse noise. First, we introduced a Gaussian mixture (GM) model to represent the statistical distribution of the received DME interference superimposed to AWGN. Then, we optimized the detection scheme of OFDM signals in GM interference to cancel the effects of DME interference. We showed that the maximum likelihood (ML) detector leads to sphere decoding under perfect knowledge of DME pulses affected observations. To support the receiver with such knowledge, we developed a simple DME pulse detector, which identifies the locations of DME samples from the received OFDM symbol. In this approach, we extracted a reference signal of the interference by utilizing the null subcarriers of L-DACS1. We presented simulation results showing that the optimum design of the L-DACS1 receiver outperforms other mitigation schemes.

Acknowledgment

This work is funded by the German Research Foundation (Deutsche Forschungsgemeinschaft, DFG).

References

[1] R. Jain, F. Templin, and Kwong-Sang Yin, "Analysis of L-Band Digital Aeronautical Communication Systems: L-DACS1 and L-DACS2," in *Aerospace Conference, 2011 IEEE*, March 2011, pp. 1–10.

[2] U. Epple, S. Brandes, S. Gligorevic, and M. Schnell, "Receiver optimization for l-dacs1," in *2009 IEEE/AIAA 28th Digital Avionics Systems Conference*, Oct. 2009.

[3] S. V. Zhidkov, "Performance analysis and optimization of ofdm receiver with blanking nonlinearity in impulsive noise environment," *IEEE Transactions on Vehicular Technology*, vol. 55, no. 1, Jan. 2006.

[4] S. V. Zhidkov, "Impulsive noise suppression in ofdm-based communication systems," *IEEE Transactions on Consumer Electronics*, vol. 49, no. 4, Nov. 2003.

[5] M. Korki, N. Hosseinzadeh, and T. Moazzeni, "Performance evaluation of a narrowband power line communication for smart grid with noise reduction technique," *IEEE Transactions on Consumer Electronics*, vol. 57, no. 4, pp. 1598–1606, November 2011.

[6] U. Epple, K. Shibli, and M. Schnell, "Investigation of blanking nonlinearity in ofdm systems," in *2011 IEEE International Conference on Communications (ICC)*, June 2011.

[7] U. Epple and M. Schnell, "Adaptive threshold optimization for a blanking nonlinearity in ofdm receivers," in *2012 IEEE Global Communications Conference (GLOBECOM)*, Dec. 2012, pp. 3661–3666.

[8] M. Raja, A. P. Vinod, and A. S. Madhukumar, "DME interference mitigation for LDACS1 based on decision-directed noise estimation," in *Integrated Communication, Navigation, and Surveillance Conference*, 2015.

[9] M. Schnell, S. Brandes, S. Gligorevic, M. Walter, C. Rihacek, M. Sajatovic, and B. Haindl, "Interference mitigation for broadband l-dacs," in *2008 IEEE/AIAA 27th Digital Avionics Systems Conference*, Oct. 2008.

[10] K. A. Saaifan and W. Henkel, "Lattice signal sets to combat pulsed interference from aeronautical signals," in *2011 IEEE International Conference on Communications (ICC)*, June 2011.

[11] J. Lin, M. Nassar, and B. L. Evans, "Impulsive noise mitigation in powerline communications using sparse bayesian learning," *IEEE Journal on Selected Areas in Communications*, vol. 31, no. 7, pp. 1172–1183, July 2013.

[12] M. Korki, J. Zhang, C. Zhang, and H. Zayyani, "Block-sparse impulsive noise reduction in ofdm systems – a novel iterative bayesian approach," *IEEE Transactions on Communications*, vol. 64, no. 1, pp. 271–284, Jan. 2016.

[13] Jurgen Haring and A. J. H. Vinck, "Iterative decoding of codes over complex numbers for impulsive noise channels," *IEEE Transactions on Information Theory*, vol. 49, no. 5, pp. 1251–1260, May 2003.

[14] K. A. Saaifan and W. Henkel, "Lattice Decoding for Multicarrier Systems in Impulse Noise," *IEEE Transactions on Communications*, Submitted.

[15] S. Brandes, U. Epple, S. Gligorevic, M. Schnell, B. Haindl, and M. Sajatovic, "Physical layer specification of the l-band digital aeronautical communications system (l-dacs1)," in *2009 Integrated Communications, Navigation and Surveillance Conference*, May 2009, pp. 1–12.

[16] N. Schneckenburger, T. Jost, D. Shutin, M. Walter, T. Thiasiriphet, M. Schnell, and U. C. Fiebig, "Measurement of the l-band air-to-ground channel for positioning applications," *IEEE Transactions on Aerospace and Electronic Systems*, vol. 52, no. 5, pp. 2281–2297, October 2016.

[17] S. Brandes, S. Gligorevic, M. Ehammer, T. Grüpl, C. H. Rokitansky, R. Dittrich, M. Schnell, and C. Rihacek, "Expected B-AMC System Performance," Tech. report, DLR, 2007.

[18] J. Miller and J. Thomas, "The detection of signals in impulsive noise modeled as a mixture process," *IEEE Transactions on Communications*, vol. 24, no. 5, pp. 559–563, May 1976.

[19] D. Andrews and C. Mallows, "Scale mixtures of normal distributions," *Journal of the Royal Statistical Society, Series B*, vol. B-36, pp. 99–102, 1974.

[20] K. Vastola, "Threshold detection in narrow-band non-Gaussian noise," *IEEE Transactions on Communications*, vol. COM-32, no. 2, pp. 134–139, February 1984.

[21] D. Middleton, "Non-Gaussian noise models in signal processing for telecommunications: new methods and results for Class-A and Class-B noise models," *IEEE Transactions on Information Theory*, vol. 45, no. 4, pp. 1129–1149, May 1999.

[22] T. Shongwe, A. J. H. Vinck, and H. C. Ferreira, "A study on impulse noise and its models," *SAIEE Africa Research Journal*, vol. 106, no. 3, pp. 119–131, 2015.

[23] U. Epple and M. Schnell, "Overview of interference situation and mitigation techniques for ldacs1," in *2011 IEEE/AIAA 30th Digital Avionics Systems Conference*, Oct. 2011.

[24] Gyemin Lee and Clayton Scott, "EM algorithms for multivariate Gaussian mixture models with truncated and censored data," *Computational Statistics & Data Analysis*, vol. 56, no. 9, pp. 2816–2829, September 2012.

[25] S. Brandes and M. Schnell, "Interference Mitigation for the Future Aeronautical L-Band Communication System," in *Multi-Carrier Systems & Solutions 2009*, 2009, vol. 41, pp. 375–384.
[26] M. O. Damen, H. El Gamal, and G. Caire, "On Maximum-Likelihood Detection and the Search for the Closest Lattice Point," *IEEE Transaction on Information Theory*, vol. 49, no. 10, pp. 2389–2402, 2003.
[27] Z. Guo and P. Nilsson, "Algorithm and implementation of the K-Best sphere decoding for MIMO detection," *IEEE Journal on Selected Aera In Communications*, vol. 24, no. 3, pp. 491–503, 2006.
[28] K.-W. Wong, C.-Y. Tsui, R. S.-K. Cheng, and W.-H. Mow, "A VLSI architecture of a K-best lattice decoding algorithm for MIMO channels," in *IEEE International Symposium on Circuits and Systems*, May 2002.

Khodr A. Saaifan Khodr Saaifan was born in Lebanon, in 1978. He received his B.Sc. and M.Sc. degree in communications from Benha and Cairo Universities in June 2001 and May 2005, respectively. In January 2015, he received his Ph.D degree (with distinction) from Jacobs University Bremen. From 2005 to 2009 he was with the Research and Development Department of wireless phones and terminals at the Egyptian Telephone Company. From 2009 to 2015, he joined the Transmission System Group (TrSys) as a research associate dealing with interference cancellation for wireless channels with a focus on MIMO systems, OFDM, and spread spectrum. Since Sept. 2015, Khodr is a postdoctoral fellow at Jacobs University Bremen. Publications are in the areas of CDMA/multiuser systems, interference modeling, impulse noise, single- and multicarrier transmission, and MIMO systems. Current research activities have a focus on coding, MIMO systems, impulse noise, and multicarrier modulation.

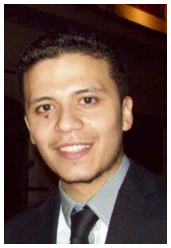

Ahmed M. Elshahed Ahmed was born in Giza, Egypt, in 1987. He received his B.Sc. degree in Electronics and Communication Engineering from Cairo University in June 2010. In March 2016, he received his M.SC degree from Jacobs University Bremen. From 2011 to 2013 he was working in the Telecoumication industry as a Radio Network Engineer at Telecomx-Consult and Vodafone Egypt, respectively. From 2013 to 2016 he moved to Jacobs University Bremen as a master student in the department of Communication, System and Electronics engineering. He joined the Transmission System Group (TrSys) at Jacobs University as Master Thesis student. Currently, he is working as Modem testing & Performance Engineer at Qualcomm CDMA Technologies.

Werner Henkel Werner Henkel was born in Gelnhausen, Germany, in 1960. He received his Diploma and Dr.-Ing. (Ph.D.) degree from Darmstadt University of Technology (TUD) in May 1984 and June 1989, respectively. From 1989 to 1999 he was with Deutsche Telekom's R&D Labs in Darmstadt and on sabbatical leave at AT&T Bell Laboratories (later Lucent) in 1993/94. From 1999 to 2002 he was with the newly founded Telecommunications Research Center Vienna, heading a basic research group dealing with access technologies with a focus on signal processing and coding for DSL. In August 2002, Dr. Henkel was appointed professor for telecommunications at the University of Applied Sciences in Bremen. Since September 2003 he is a professor for electrical engineering at the Jacobs University Bremen. Earlier teaching obligations were at University of Kaiserslautern and TU Vienna.
He was a guest editor for the June 2002 issue of IEEE J-SAC. He was in the program/organizating committees of ISIT 1997, the International Zürich Seminar 2004, of EUSIPCO 2004 and 2007, ICC 2006, and of the Turbo Symposia 2008, 2010, and 2014. Publications are in the areas of coding, iterative decoding, coded modulation, network coding, frame synchronization, channel modeling, impulse noise, DSL, single- and multicarrier transmission, and MIMO/multiuser systems. Current research activities have a focus on unequal error protection in networking, coding, and physical layer, multicarrier transmission, MIMO and multiuser systems, iterative decoding, channel measurement and modeling, and gene coding.